

Ultrastrong adhesion of graphene membranes

Steven P. Koenig, Narasimha G. Boddeti, Martin L. Dunn and J. Scott Bunch*

As mechanical structures enter the nanoscale regime, the influence of van der Waals forces increases. Graphene is attractive for nanomechanical systems^{1,2} because its Young's modulus and strength are both intrinsically high, but the mechanical behaviour of graphene is also strongly influenced by the van der Waals force^{3,4}. For example, this force clamps graphene samples to substrates, and also holds together the individual graphene sheets in multilayer samples. Here we use a pressurized blister test to directly measure the adhesion energy of graphene sheets with a silicon oxide substrate. We find an adhesion energy of $0.45 \pm 0.02 \text{ J m}^{-2}$ for monolayer graphene and $0.31 \pm 0.03 \text{ J m}^{-2}$ for samples containing two to five graphene sheets. These values are larger than the adhesion energies measured in typical micromechanical structures and are comparable to solid-liquid adhesion energies⁵⁻⁷. We attribute this to the extreme flexibility of graphene, which allows it to conform to the topography of even the smoothest substrates, thus making its interaction with the substrate more liquid-like than solid-like.

Optical images of the devices used for this study are shown in Fig. 1a. Graphene-sealed microcavities were fabricated by the mechanical exfoliation of graphene over predefined microcavities (diameter, $\sim 5 \mu\text{m}$) etched in a SiO_2 substrate (see Methods). Two exfoliated graphene flakes were used, yielding membranes with between one and five graphene layers, which were suspended over the microcavities and clamped to the SiO_2 substrate by the van der Waals force. After exfoliation, the internal pressure in the microcavity, p_{int} , is equal to the external pressure, p_{ext} (atmospheric pressure). In this state, the membrane is flat and adhered to the substrate, and confines nitrogen gas molecules inside the microcavity.

To create a pressure difference across the graphene membrane, we placed the sample in a pressure chamber and used nitrogen gas to increase p_{ext} to p_0 . Devices were left in the pressure chamber at p_0 for between four and six days to allow p_{int} to equilibrate to p_0 (Fig. 1b). This is thought to take place through the slow diffusion of gas through the SiO_2 substrate³. We then removed the device from the pressure chamber, whereupon the pressure difference ($p_{\text{int}} > p_{\text{ext}}$) caused the membrane to bulge upwards and the volume of the microcavity to increase (Fig. 1c). An atomic force microscope (AFM) was used to measure the shape of the graphene membrane, which we parameterize by its maximum deflection δ and its radius a (Fig. 1c).

This technique allows us to measure δ and a for different values of p_0 . Figure 1e shows a series of AFM line cuts through the centre of a monolayer membrane as p_0 is increased. At low p_0 , the membrane is clamped to the substrate by the van der Waals force, and δ increases with increasing p_0 . At higher p_0 (for example, $p_0 > 2 \text{ MPa}$), in addition to an increased deflection, we also observe delamination of the graphene from the SiO_2 substrate, leading to an increase in a (Fig. 1e). In Fig. 2a, we plot the maximum deflection δ versus p_0 for all measured bilayer membranes (results are similar for other devices; see Supplementary Information). The deflection increases nonlinearly until $p_0 \approx 2.5 \text{ MPa}$, and δ then begins to increase more rapidly. The blister radius stays constant until $p_0 \approx 2.5 \text{ MPa}$ and then abruptly increases with increasing p_0 (Fig. 2b).

At large p_0 (for example, $> 3.0 \text{ MPa}$), stable delamination occurs, with a increasing and thus Δp decreasing with increasing p_0 (Fig. 2c). All of the pressurized graphene membranes show a great degree of axisymmetry in their deformation before and after delamination. Stable delamination is in stark contrast to the common constant pressure blister test, which results in unstable crack growth at the onset of delamination⁸. As a result, we call this the 'constant N blister test', because the number of molecules in the microcavity is constant during blister delamination. Although a macroscopic counterpart of the constant N blister test has been demonstrated⁹ (although not widely used), the novelty here is in the use of the adhesion between graphene and SiO_2 to prepare an impermeable seal for gas in the microcavity—filling and emptying of the microcavity are accomplished by diffusion through the SiO_2 , which is slow enough to allow reliable measurements of stable delamination³.

We use the measured membrane profile (deflection δ and blister radius a versus p_0) in the constant N blister test to determine the graphene/ SiO_2 adhesion energy. To this end, we describe the deformation of the membrane using Hencky's solution^{10,11} for the geometrically nonlinear response of a clamped isotropic circular elastic membrane subjected to a pressure difference Δp across the membrane. This solution provides the membrane profile in the form of an infinite series in radial position, and also the relationship between the pressure difference and blister height, $\Delta p = K(\nu)(E t \delta^3)/a^4$, and the volume of the blister $V_b(a) = C(\nu)\pi a^2 \delta$. Here, E is Young's modulus, ν is Poisson's ratio, t is the membrane thickness, and $C(\nu)$ and $K(\nu)$ are coefficients that depend only on ν and vary from $K(\nu = 0.10) = 2.93$ to $K(\nu = 0.20) = 3.22$. The $K(\nu)\delta^3/a^4$ term primarily describes the geometrical nonlinear deflection-pressure response of the circular membrane, as $K(\nu)$ is a coefficient that is fixed for a specified ν . For graphene, we take $\nu = 0.16$ (ref. 12) and so $K(\nu = 0.16) = 3.09$ and $C(\nu = 0.16) = 0.524$.

To determine the adhesion energy we model the constant N blister as a thermodynamic system with free energy:

$$F = \frac{(p_{\text{int}} - p_{\text{ext}})V_b}{4} + \Gamma\pi(a^2 - a_0^2) - p_0 V_0 \ln\left(\frac{V_0 + V_b}{V_0}\right) + p_{\text{ext}} V_b \quad (1)$$

where V_0 is the initial volume of the microcavity, Γ is the graphene/ SiO_2 adhesion energy, and a_0 is the initial radius before delamination⁹. In equation (1) the four terms represent, respectively, (1) stretching of the membrane due to the pressure difference across it, $\Delta p = p_{\text{int}} - p_{\text{ext}}$ (we calculate this by equating the strain energy in the deformed membrane to the work done by the expanding gas during deformation, which is easier to directly calculate, and then simplifying the results using Hencky's relations for the pressure-deflection and pressure-blister volume); (2) graphene/ SiO_2 adhesion; (3) expansion of the gas in the chamber from V_0 to a final volume $V_0 + V_b(a)$; and (4) work done on the gas held at a fixed external pressure p_{ext} . To deduce Δp across the membrane we use the ideal gas law and assume isothermal expansion of the

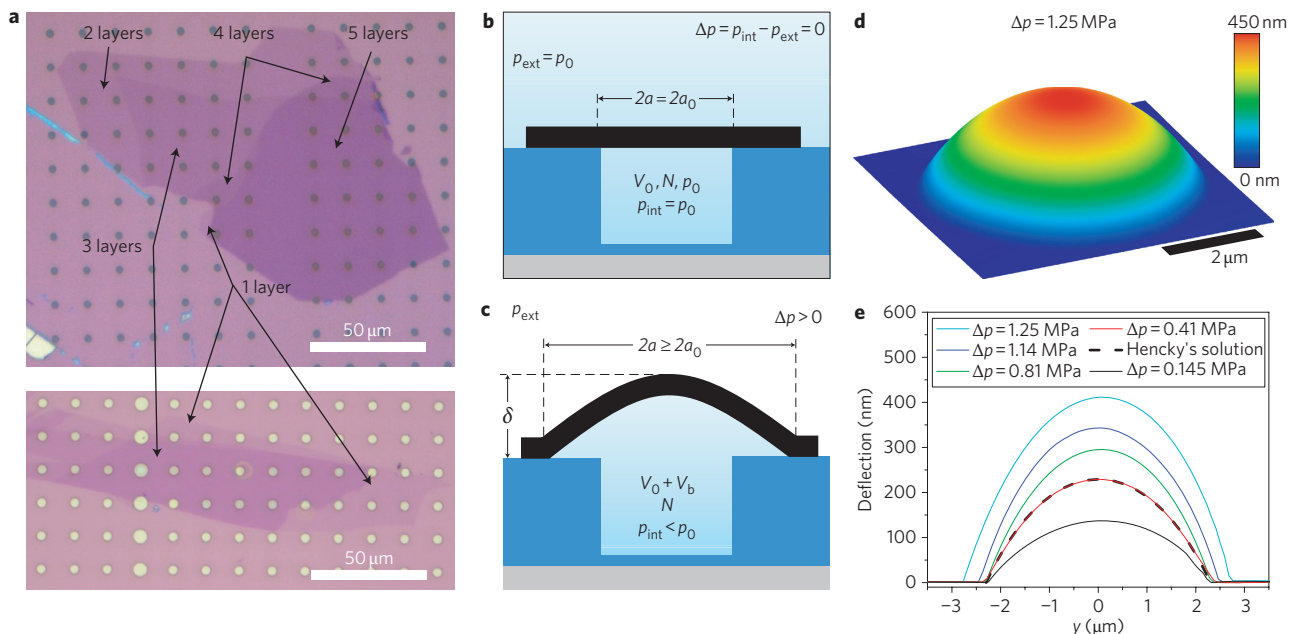


Figure 1 | Pressurizing graphene membranes. **a**, Two optical images showing graphene flakes with regions of one to five suspended layers (top), and one and three suspended layers (bottom). The arrays of microcavities in the SiO₂ substrate can also be seen. The number of graphene layers was verified with a combination of Raman spectroscopy, AFM and measurements of optical contrast and elastic constants measurements (see Supplementary Information). **b**, Schematic of a graphene-sealed microcavity before it is placed in the pressure chamber. The pressure inside the microcavity, p_{int} , is equal to the external pressure p_{ext} , so the membrane is flat. After four to six days inside the pressure chamber, p_{int} increases to p_0 . **c**, When the microcavity is removed from the pressure chamber, the pressure difference across the membrane causes it to bulge upward and eventually delaminate from the substrate, causing the radius a to increase. **d**, Three-dimensional rendering of an AFM image showing the deformed shape of a monolayer graphene membrane with $\Delta p = p_{\text{int}} - p_{\text{ext}} = 1.25$ MPa. **e**, Deflection versus position for five different values of Δp between 0.145 MPa (black) and 1.25 MPa (cyan). The dashed black line is obtained from Hencky's solution for $\Delta p = 0.41$ MPa. The deflection is measured by AFM along a line that passes through the centre of the membrane.

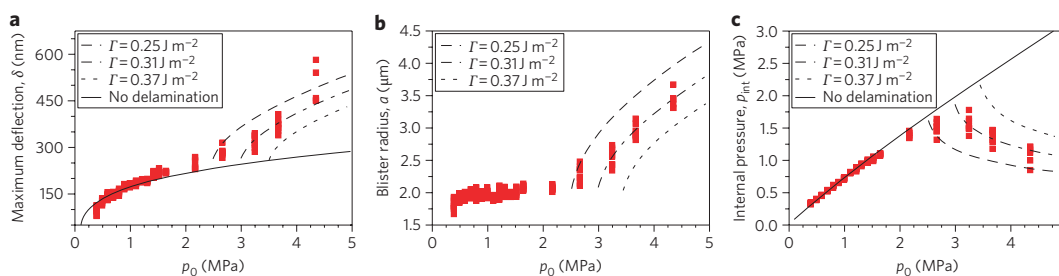


Figure 2 | Delaminating graphene membranes. **a-c**, Plots showing maximum deflection δ (**a**), blister radius a (**b**) and internal pressure p_{int} (**c**) versus input pressure p_0 for all two-layer membranes studied. The solid black line is a theoretical curve assuming no delamination of the membrane. Dashed lines are theoretical curves for $nEt = 694$ N m⁻¹, $n = 2$ and three different values of the graphene/SiO₂ adhesion energy Γ .

trapped gas (see Methods). Minimizing the free energy with respect to a provides a relationship between Γ , δ and a :

$$\Gamma = \frac{5C}{4} \left(p_0 \frac{V_0}{V_0 + V_b(a)} - p_{\text{ext}} \right) \delta \quad (2)$$

We use equation (2) to determine Γ with prescribed values of p_0 and p_{ext} , (a , δ) pairs measured by AFM, V_0 determined by the microcavity geometry, and $V_b(a)$. Values of adhesion energy extracted in this manner are shown for all devices in Fig. 3. The value $\Gamma = 0.31 \pm 0.03$ J m⁻² describes the multilayer graphene/SiO₂ adhesion reasonably well for both SiO₂ substrates used in this study, but not the monolayer, which has a value of 0.45 ± 0.02 J m⁻² (see Supplementary Information).

Our measured adhesion energies are approximately four orders of magnitude larger than adhesion energies commonly found in micro-mechanical systems, where van der Waals forces across non-contacting regions between asperities play a significant role, and

approximately five times larger than adhesion in gold-coated sub-micrometre beams^{5,7,13-15}. They are also twice previous estimates for multilayer graphene and a SiO₂ substrate¹⁶; however, those results were extracted from a model that uses an estimate of Young's modulus of graphene that is one-half of that measured here. Our results are comparable to values deduced from experiments on collapsed carbon nanotubes¹⁷. Using values derived from the measured surface energies of graphite ($\gamma = 165$ – 200 mJ m⁻²) and SiO₂ ($\gamma = 115$ – 200 mJ m⁻²), one expects an adhesion energy of $\Gamma = 2 (\gamma_{\text{SiO}_2} \times \gamma_{\text{graphite}})^{1/2} = (0.275$ – $0.4)$ J m⁻² (refs 6,17). The close agreement between our measured adhesion energy and this estimate suggests that graphene makes close and intimate contact with the SiO₂ substrate^{18,19}. It shows that atomically thin structures such as graphene demonstrate conformation over the SiO₂ surface that is more reminiscent of a liquid than a solid.

The reason for the higher adhesion of monolayer graphene than multilayer graphene is not entirely understood. We ruled out

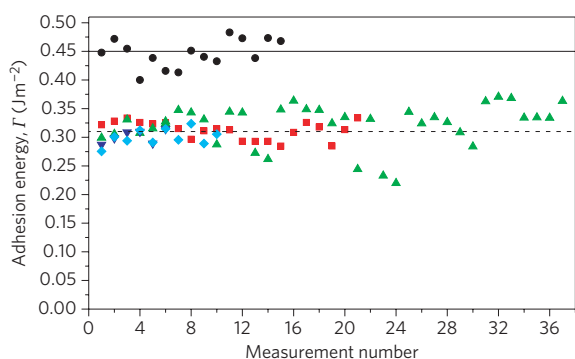


Figure 3 | Graphene/SiO₂ adhesion energies. Measured adhesion energies Γ for membranes containing one layer of graphene (black circles), two layers (red squares), three layers (green triangles), four layers (blue triangles) and five layers (cyan diamonds). The upper solid line corresponds to $\Gamma = 0.45 \text{ J m}^{-2}$ and the lower dashed line corresponds to $\Gamma = 0.31 \text{ J m}^{-2}$.

bonding due to induced image charges from buried charges in the SiO₂ substrate (see Supplementary Information). A possible explanation for the discrepancy between graphene with one and two to five layers is the increased ability of monolayer graphene to conform to the contours of the surface as a result of its flexibility. Roughness measurements of various layers of graphene on the SiO₂ substrate taken with the AFM show a decreasing roughness with increasing layer number (~197 pm for bare SiO₂, 185 pm with one layer, and 127 pm with 15 layers of graphene) suggesting that monolayer graphene conforms more closely to the SiO₂ substrate (see Supplementary Information). Recent theory that idealizes the substrate roughness as a sinusoidal profile shows a jump in adhesion energy with wavelength and amplitude^{20–22}. We modified this theory to account for effects of multilayer graphene, and it supports the suggestion of a jump to contact that results in increased adhesion energy as the number of layers decreases; however, the model is too simple to quantitatively predict that this jump occurs between $n = 2$ and 1 layers.

As mentioned, the deformation of the membrane can be described using Hencky’s solution for the geometrically nonlinear response of a clamped circular elastic membrane subjected to a

pressure difference Δp across the membrane. The dashed line in Fig. 1e compares the calculated profile using Hencky’s solution^{10,11} with our measured profile. The close agreement validates the use of a and δ to parameterize the deformation. Figure 2c shows the equilibrium p_{int} versus p_0 for the bilayer devices. The solid lines in Fig. 2a and c are the solutions of

$$\Delta p = K(v)(Et\delta^3)/a^4 \tag{3}$$

for a constant $a = a_0$ (no delamination) where we used the fitted value of Et . This provides a good fit until delamination begins ($a > a_0$) at $p_0 = 2.5 \text{ MPa}$ (Fig. 2b). The dashed lines in Fig. 2 are theoretical predictions of δ , a and p_{int} versus p_0 using the average adhesion energy values from Fig. 3 and the fitted value of Et .

Figure 4a shows $K(v)\delta^3/a^4$ versus Δp for the monolayer graphene membrane and also a linear fit to equation (3) to determine $Et = 347 \text{ N m}^{-1}$. This agrees well with previous measurements for graphene and the in-plane modulus ($E = 1 \text{ TPa}$) and interatomic spacing of graphite ($t = 0.335 \text{ nm}$)^{3,4,12}. Figure 4b–e shows $K(v)\delta^3/a^4$ versus Δp for membranes containing two to five graphene sheets. Included are linear fits to the data for $\Delta p < 0.50 \text{ MPa}$ (dashed lines). Theoretical estimates with nEt (solid lines) where $Et = 347 \text{ N m}^{-1}$ (our monolayer measurement) and $n = 1–5$ (corresponding to the number of graphene layers) are also plotted, and the Et values obtained by both methods are compared in Fig. 4f. The good agreement between these values demonstrates that the additional graphene layers are sufficiently well adhered to the substrate and each other by the van der Waals force so that the pressure load is carried by all the layers and no significant sliding or delamination occurs up to pressures as large as $\Delta p = 0.50 \text{ MPa}$ (refs 23,24). For $\Delta p < 0.25 \text{ MPa}$ the effect of initial tension in the membrane cannot be neglected and for $\Delta p > 0.50 \text{ MPa}$ the data show considerably more scatter (see Supplementary Information). Further work is necessary to understand the origin of this scatter, but two possibilities are small amounts of sliding or early stages of delamination, which are difficult to measure by AFM.

In conclusion, we have demonstrated a simple yet reliable constant N blister test and used it to measure the adhesion energy of the thinnest

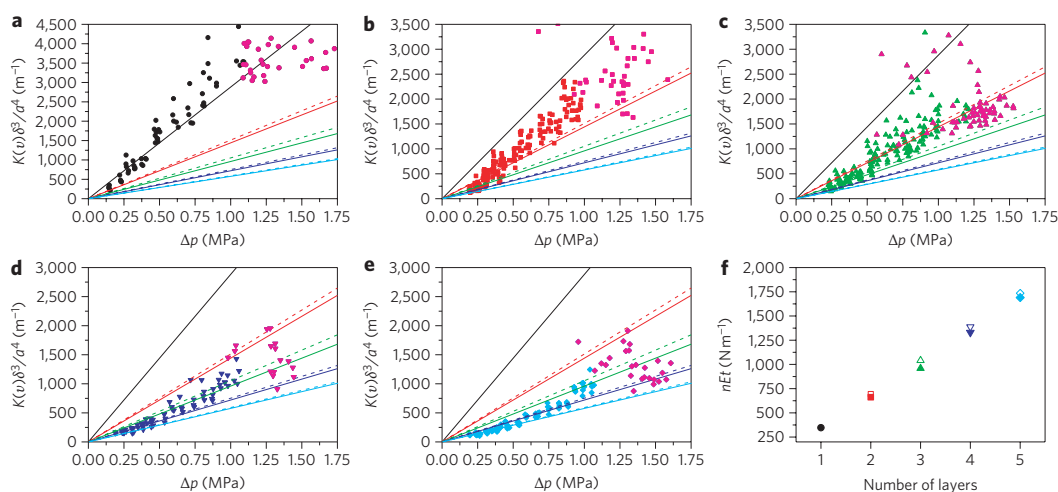


Figure 4 | Elastic constants and clamping of graphene membranes. **a–e**, $K(v)\delta^3/a^4$ versus pressure difference Δp for membranes containing one graphene sheet before delamination (black symbols) and after delamination (magenta). **b–e**, Same plot as **a** for membranes containing two (red symbols), three (green), four (blue) or five (cyan) sheets of graphene before and after delamination (magenta symbols in all plots). The solid lines are linear fits to all the data with $nEt = 347$ (black), 694 (red), 1,041 (green), 1,388 (blue) and 1,735 N m^{-1} (cyan) (n , number of graphene sheets; E , Young’s modulus; t , membrane thickness). Dashed lines show linear fits to the data for $\Delta p < 0.50 \text{ MPa}$ and have slopes corresponding to $Et = 661$ (red; two layers), 950 (green; three layers), 1,330 (red; four layers) and 1,690 N m^{-1} (cyan; five layers). Note that the vertical scales are different. **f**, nEt versus number of layers. Solid symbols are fitted lines; open symbols indicate nEt , with $Et = 347$.

nanostructures possible, single and multilayer graphene sheets, to SiO₂. This is the first direct measurement of the adhesion energy of one-to-five-layer graphene to SiO₂, a substrate on which the majority of graphene electrical and mechanical devices are fabricated. This result can be used to guide developments in graphene-based electrical and mechanical devices where adhesive forces are known to have an important role, and it should also provide opportunities for fundamental studies of surface forces in the thinnest structures possible^{3,25–28}

Methods

Suspended graphene membranes were fabricated by a combination of standard photolithography and mechanical exfoliation of graphene. An array of circles with diameters of 5 and 7 μm was first defined by photolithography on an oxidized silicon wafer with a silicon oxide thickness of 285 nm. Reactive ion etching was then used to etch the circles into cylindrical microcavities with a depth of 250–300 nm, leaving a series of microcavities on the wafer. Mechanical exfoliation of natural graphite using Scotch tape was then used to deposit suspended graphene sheets over the microcavities²⁹. Of the 39 membranes there were 5 one-layer, 10 two-layer, 15 three-layer, 4 four-layer, and 5 five-layer membranes. The number of graphene layers was verified using a combination of Raman spectroscopy, optical contrast, AFM measurements, and elastic constants measurements (see Supplementary Information)^{30,31}. Two flakes on two different SiO₂ substrates were used in this study (Fig. 1a). Three two-layer membranes, 4 three-layer membranes and 1 four-layer membrane were damaged before reaching the highest pressures.

To deduce $\Delta p = p_{\text{int}} - p_{\text{ext}}$ across the membrane we used the ideal gas law and assume isothermal expansion of the trapped gas with a constant number of molecules, N . Doing so led to $p_0 V_0 = p_{\text{int}} (V_0 + V_b)$, where V_0 is the initial volume of the microcavity and V_b is the volume of the pressurized blister after the device is brought to atmospheric pressure and bulges upward. The assumption of constant N is valid considering that the deflection does not change over the ~20 min that the AFM images are acquired, suggesting that no significant change in N , due to gas 'leaking', occurs on the timescale of the experiment.

Received 13 May 2011; accepted 30 June 2011;
published online 14 August 2011

References

- Bunch, J. S. *et al.* Electromechanical resonators from graphene sheets. *Science* **315**, 490–493 (2007).
- Meyer, J. C. *et al.* The structure of suspended graphene sheets. *Nature* **446**, 60–63 (2007).
- Bunch, J. S. *et al.* Impermeable atomic membranes from graphene sheets. *Nano Lett.* **8**, 2458–2462 (2008).
- Lee, C. *et al.* Measurement of the elastic properties and intrinsic strength of monolayer graphene. *Science* **321**, 385–388 (2008).
- Maboudian, R. & Howe, R. T. Critical review: adhesion in surface micromechanical structures. *J. Vac. Sci. Technol. B* **15**, 1–20 (1997).
- Israelachvili, J. *Intermolecular and Surface Forces* (Academic Press, 2011).
- Delrio, F. W. *et al.* The role of van der Waals forces in adhesion of micromachined surfaces. *Nature Mater.* **4**, 629–634 (2005).
- Gent, A. N. & Lewandowski, L. H. Blow-off pressures for adhering layers. *J. Appl. Polym. Sci.* **33**, 1567–1577 (1987).
- Wan, K. & Mai, Y. Fracture mechanics of a new blister test with stable crack growth. *Acta Metall. Mater.* **43**, 4109–4115 (1995).
- Hencky, H. Über den Spannungszustand in kreisrunden platten mit verschwindender biegungssteifigkeit. *Z. fur Mathematik und Physik* **63**, 311–317 (1915).
- Williams, J. Energy release rates for the peeling of flexible membranes and the analysis of blister tests. *Int. J. Fracture* **87**, 265–288 (1997).
- Blakslee, O. L. *et al.* Elastic constants of compression-annealed pyrolytic graphite. *J. Appl. Phys.* **41**, 3373–3382 (1970).
- DelRio, F. W. *et al.* The effect of nanoparticles on rough surface adhesion. *J. Appl. Phys.* **99**, 104304 (2006).
- DelRio, F. W. *et al.* Elastic and adhesive properties of alkanethiol self-assembled monolayers on gold. *Appl. Phys. Lett.* **94**, 131909 (2009).
- Buks, E. & Roukes, M. L. Stiction, adhesion energy, and the Casimir effect in micromechanical systems. *Phys. Rev. B* **63**, 33402 (2001).
- Zong, Z. *et al.* Direct measurement of graphene adhesion on silicon surface by intercalation of nanoparticles. *J. Appl. Phys.* **107**, 026104 (2010).
- Yu, M. F., Kowalewski, T. & Ruoff, R. S. Structural analysis of collapsed, and twisted and collapsed, multiwalled carbon nanotubes by atomic force microscopy. *Phys. Rev. Lett.* **86**, 87–90 (2001).
- Cullen, W. *et al.* High-fidelity conformation of graphene to SiO₂ topographic features. *Phys. Rev. Lett.* **105**, 215504 (2010).
- Rudenko, A. N. *et al.* Local interfacial interactions between amorphous SiO₂ and supported graphene. Preprint at <http://arxiv.org/abs/1105.1655> (2011).
- Aitken, Z. H. & Huang, R. Effects of mismatch strain and substrate surface corrugation on morphology of supported monolayer graphene. *J. Appl. Phys.* **107**, 123531 (2010).
- Li, T. & Zhang, Z. Substrate-regulated morphology of graphene. *J. Phys. D* **43**, 075303 (2010).
- Kusminskiy, S. V. *et al.* Pinning of a two-dimensional membrane on top of a patterned substrate: the case of graphene. *Phys. Rev. B* **83**, 165405 (2011).
- Suk, J. W. *et al.* Mechanical properties of monolayer graphene oxide. *ACS Nano* **4**, 6557–6564 (2010).
- Ruiz-Vargas, C. S. *et al.* Softened elastic response and unzipping in chemical vapor deposition graphene membranes. *Nano Lett.* **11**, 2259–2263 (2011).
- Lee, C. *et al.* Frictional characteristics of atomically thin sheets. *Science* **328**, 76–80 (2010).
- Lui, C. H. *et al.* Ultraflat graphene. *Nature* **462**, 339–341 (2009).
- Capasso, F. *et al.* Casimir forces and quantum electrodynamic torques: physics and nanomechanics. *IEEE J. Sel. Top. Quant.* **13**, 400–414 (2007).
- Lu, Z. & Dunn, M. L. van der Waals adhesion of graphene membranes. *J. Appl. Phys.* **107**, 044301 (2010).
- Novoselov, K. S. *et al.* Two-dimensional atomic crystals. *Proc. Natl Acad. Sci. USA* **102**, 10451–10453 (2005).
- Koh, Y. K. *et al.* Reliably counting atomic planes of few-layer graphene ($n > 4$). *ACS Nano* **5**, 269–274 (2011).
- Ferrari, A. C. *et al.* Raman spectrum of graphene and graphene layers. *Phys. Rev. Lett.* **97**, 187401 (2006).

Acknowledgements

This work was supported by the National Science Foundation (NSF, grant nos. 0900832 and 1054406), the NSF Industry/University Cooperative Research Center for Membrane Science, Engineering and Technology at the University of Colorado at Boulder, and the DARPA Center on Nanoscale Science and Technology for Integrated Micro/Nano-Electromechanical Transducers (DARPA/SPAWAR, grant no. N66001-10-1-4007). Sample fabrication was performed at the University of Colorado node of the National Nanofabrication Users Network, funded by the NSF. The authors thank G. Acosta, L. Wang and X. Liu for help with fabrication and R. Raj for use of the Raman microscope.

Author contributions

S.P.K. performed the experiments. S.P.K. and J.S.B. conceived and designed the experiments. N.G.B. and M.L.D. developed the theory and modelling. All authors interpreted the results and co-wrote the manuscript.

Additional information

The authors declare no competing financial interests. Supplementary information accompanies this paper at www.nature.com/naturenanotechnology. Reprints and permission information is available online at <http://www.nature.com/reprints>. Correspondence and requests for materials should be addressed to J.S.B.